

UNCLASSIFIED

Defense Technical Information Center
Compilation Part Notice

ADP014041

TITLE: Doppler Properties of Airborne Clutter

DISTRIBUTION: Approved for public release, distribution unlimited
Availability: Hard copy only.

This paper is part of the following report:

TITLE: Military Application of Space-Time Adaptive Processing [Les applications militaires du traitement adaptatif espace-temps]

To order the complete compilation report, use: ADA415645

The component part is provided here to allow users access to individually authored sections of proceedings, annals, symposia, etc. However, the component should be considered within the context of the overall compilation report and not as a stand-alone technical report.

The following component part numbers comprise the compilation report:

ADP014040 thru ADP014047

UNCLASSIFIED

Doppler Properties of Airborne Clutter

Richard Klemm

FGAN-FHR, Neuenahrer Str. 20, D 53343 Wachtberg, Germany
Tel +49 228 9435 377; Fax +49 228 9435 618; email r.klemm@fgan.de

Abstract

Detection of slowly moving targets by air- and spaceborne MTI radar is heavily degraded by the motion induced Doppler spread of clutter returns. Space-time adaptive processing (STAP) can achieve optimum clutter rejection via implicit platform motion compensation. In this report the fundamentals and properties of STAP applied to air- and spaceborne MTI radar are summarised. The effect of platform motion on the characteristics of airborne clutter is discussed. The performance of the optimum space-time processor is shown. Comparison with spatial or temporal only techniques illustrate the importance of space-time processing.

1 Introduction

The main application of space-time adaptive processing (STAP) is the suppression of clutter received by a moving radar. In this case we talk about space-slow time (pulse-to-pulse) processing. The radar platform motion causes clutter returns to be Doppler shifted. The Doppler shift is proportional to the platform velocity and the angle of arrival. The total of all clutter arrivals sums up in a Doppler broadband clutter echo. Targets whose Doppler frequencies fall into the clutter Doppler bandwidth may be difficult to detect. It should be noted that most moving targets are "slow" or low Doppler targets, either because they are slow or exhibit a low Doppler due to their motion direction. For a radar on a satellite (10 km/s) all targets near the ground (jet aircraft 300 m/s) are slow targets.

Other important techniques operate in the space-fast time (range equivalent) domain. They are used to either suppress jammers in broadband array radar or for mitigating terrain scattered jamming.

Space-time processing needs space-time data to operate on. Space-time data are obtained from a radar which has a phased array antenna with multiple outputs (spatial dimension), and transmits coherent pulse trains (temporal dimension).

1.1 The principle of adaptive clutter suppression

1.1.1 Practical application: adaptive clutter filter for surveillance radar

The following experiment conducted in the early 1970's (BÜHRING & KLEMM [6]) is described briefly to illustrate the principle of adaptive clutter filtering. This filter was designed to suppress weather clutter with unknown centre Doppler frequency and bandwidth. This adaptive MTI systems was operated with a conventional groundbased surveillance radar with rotating reflector antenna. Figure 1 shows the block diagram of an adaptive FIR filter based on the prediction error filter principle. The filter coefficients were estimated in real-time and the echo data were clutter filtered during the following revolution of the antenna.

In Figure 2 the filtering effect is demonstrated using simulated clutter. The picture shows a photograph of a PPI (pla position indicator) screen. The zero Doppler filter has been switched off so that a lot of ground clutter can be noticed. The spokes are the simulated clutter (for simplicity this clutter was simulated independent of range). The available radar operated in L-band which is quite insensitive to weather. Therefore, to have reproduceable clutter conditions a hardwired simulator was developed. The clutter filter was adapted based on clutter data in the window on the right. As can be seen the clutter has been removed and a (true) target is visible.

Figure 3 and 4 show suppression of a real weather cloud before and after filtering. Except for a few false alarms the weather clutter has been removed. The air targets (big spots on the left) did not do us the favour to enter our measurement window, they just bypass it¹.

¹No responsible pilot will enter a thunder storm deliberately.

1.2 The History of STAP

In the following two sections a brief review of the history of research and experimental work on STAP is given.

1.2.1 Theoretical work (Table 1)

Table 1 includes a number of publications which represent milestones in the evolution of STAP. This selection of papers is certainly not exhaustive but to our opinion representative. In some cases merely the earliest papers rather than the most significant papers are quoted. In the meantime special journal issues (# 20,21) and tutorials (# 12,19,20) on STAP are available.

The original idea of reducing the clutter spectrum via motion compensation originates from ANDERSON (# 1). This paper was written before digital technology was available. The DPCA technique SKOLNIK (# 2) was also originally invented for use with for implementation in microwave technology. This technique compensates physically or electronically for the platform motion in a non-adaptive fashion. The paper by BRENNAN & REED (# 3) is the basis for all future space-time processing. It deals with interference rejection in broadband arrays. This principle was analysed in some detail by COMPTON (# 7). The first paper on STAP was written by BRENNAN et al. (# 4). Here the optimum (maximum likelihood) processor applied to clutter rejection for moving radar has been described and analysed. Starting from (# 4) KLEMM discovered that the size of the clutter subspace is about $N + M$ under certain conditions which gave rise to manyfold research on subspace processor architectures (# 8, 9, 12, 13, 18, 20). Later on an extension of this result became known as "Brennan's Rule" (# 10). Problems of real-time implementation of STAP processors have been discussed by FARINA et al. (# 11). WARD (# 15) presented angle and Doppler estimation errors for STAP radar. ENDER (# 17) demonstrated the detection and re-positioning of moving targets in SAR images obtained with the multi-channel SAR AER II. DOHERTY et al. and JOUNY et al. (# 16) used STAP techniques to mitigate the effect of terrain scattered jamming. STAP in conjunction with bistatic radar has been discussed by KLEMM (# 23). A recent trend of moving reconnaissance function from airborne to space-borne platforms can be noticed (COVAULT (# 24)). Besides the STAP research activities in the USA and Europe some considerable interest of Chinese scientists in STAP can be noticed (# 6).

1.2.2 Experiments and Systems (Table 2)

In Table 2 experimental and operational STAP systems are listed. The first (non-adaptive) DPCA experiment involving an array antenna has been carried out by Tsandoulas (# 1). The NRL (# 3) and MCARM experiments (# 4) use linear sidelooking arrays. Both programs lead to many detailed investigations on possibilities of airborne clutter rejection. A large number of publications originate from these programs, dealing with various research topics such as clutter homogeneity, sidelobe Doppler clutter, knowledge-based MTI processing, subspace techniques (e.g., $\Sigma - \Delta$), and bistatic operation (# 11). The Mountaintop program (# 5) was started in 1990 to study advanced processing techniques and technologies to support the requirements of future airborne early warning radar platforms. In particular the effect of terrain scattered jamming has been studied. In Europe the AER II program (# 7, Germany), the DO-SAR experiment (# 8, Germany) and the DERA experiment (# 9, UK) have been conducted.

There are three operational systems with space-time ground clutter rejection capability (Joint STARS (# 2), AN/APG-76 (# 6), and the AN/APY-6). The first one has a 3-aperture sidelooking array antenna and has been flown in the Gulf War. The AN/APG-76 is a forward looking nose radar and the AN/APY-6 has both sidelooking and forward looking capability. From the available literature it is not obvious whether these system are based on adaptive algorithms (STAP) or used some non-adaptive DPCA-like techniques.

1.2.3 Historical note

The non-adaptive DPCA technique has been described already in SKOLNIK ed. [39]. Research on space-time *adaptive* processing started with the paper by BRENNAN et al. [4] in 1976 on space-time MTI (moving target

indication) processing for airborne radar. Very little has been published in the following years. In 1983 the author introduced the concept of eigenanalysis of the space-time clutter covariance matrix which opened the horizon towards subspace techniques for real-time applications [21]. A number of follow-up papers by the author have been concerned with various suboptimum approaches based on order reducing transforms of the signal subspace. These papers have been summarized in a book on STAP (KLEMM [26]). Since 1990 research activities on STAP increased tremendously, particularly in the USA (e.g. WARD [46], WANG & CAI [43]), in China (e.g. WANG & BAO [44]), in the UK (RICHARDSON & HAYWARD [35]), and in Italy FARINA et al. [15]).

#	year	subject	authors
1	1958	First paper on motion compensated MTI	Anderson [1]
2	1970	DPCA	Skolnik [39]
3	1973	Theory of adaptive radar	Brennan & Reed [3]
4	1976	First paper on STAP	Brennan et al. [4]
5	1983	Dimension of clutter subspace	Klemm [21]
6	≈ 1987	First Chinese papers	e.g. Wang & Bao [44]
7	1988	Broadband jammer cancellation	Compton [9, 8]
8	1990	Space-time FIR filter	Klemm & Ender [22]
9	1992	Spatial transform techniques	Klemm [23]
10	1992	Brennan's Rule	Brennan & Staudaher [5]
11	1992	Real-time implementation of STAP	Farina et al. [15]
12	1994	Report on STAP	Ward [46]
13	1994	Beam/Doppler space processing	Wang & Cai [43]
14	1995	STAP for forward looking arrays	Richardson & Hayward [35] Klemm [24]
15	1995	Angle/velocity estimation with STAP radar	Ward [47]
16	1995	Mitigation of terrain scattered jamming	Doherty [11], Jouny et al. [20]
17	1996	STAP for SAR	Ender [13]
18	1996	$\Sigma - \Delta$ STAP	Wang et al. [45]
19	1996	Effect of platform maneuvers	Richardson et al. [36]
20	1998	IEE Colloquium on STAP	Klemm (chair) [25]
21	1998	Textbook on STAP	Klemm [26]
22	1998	Effect of range walk	Kreyenkamp [33]
23	1999	IEE ECEJ special issue on STAP	Klemm (ed) [28]
24	1999	IEEE Trans. AES: Special issue on STAP and Adaptive Arrays	Melvin (ed.) [32]
25	1999	STAP with bistatic radar	Klemm [27]
26	1999	STAP for future observation satellites	Covault [10]

Table 1. Some milestones in STAP research

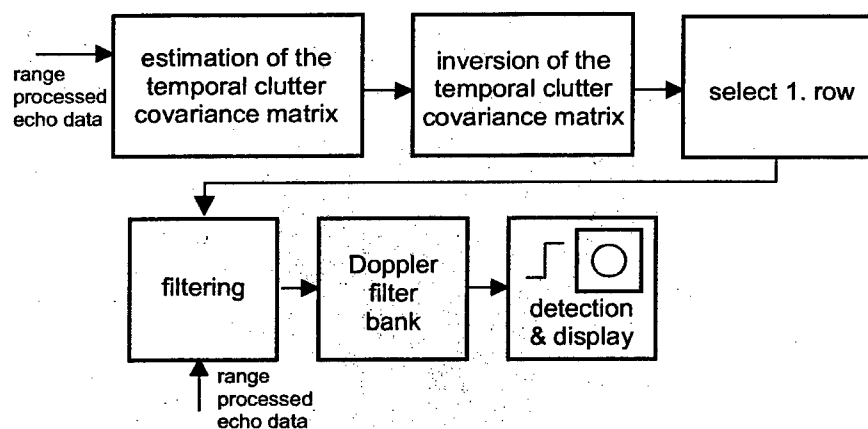


Figure 1: Block diagram of adaptive temporal clutter filter

#	year	system	authors
1	1973	DPCA with array antenna (flight experiment)	Tsandoulas [42]
2	1991	Joint STARS antenna	Shnitkin [38]
3	1992	NRL experiment	Lee & Staudaher [34]
4	1994	MCARM experiment	Babu [2]
5	1994	Mountaintop	Titi [41]
6	1996	AN/APG-76 sidelooking airborne array radar	Tobin [40]
7	1996	AER II	Ender [12]
8	1996	Dornier's DO-SAR	Hippler & Fritsch [19]
9	1996	DERA STAP experiment	Coe et al. [7]
10	1998	AN/APY-6 airborne array radar	Gross & Holt [16]
11	1999	STAP with bistatic radar	Sanyal et al. [37]

Table 2. Existing STAP systems

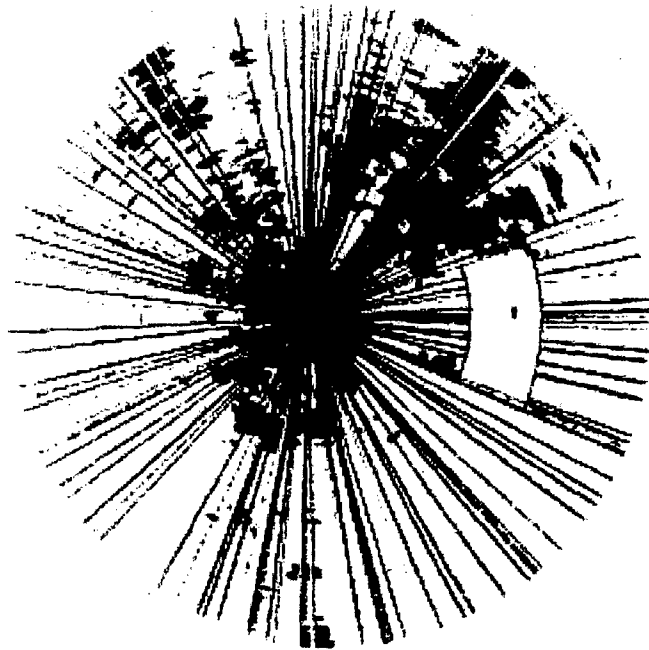


Figure 2: Adaptive suppression of simulated weather clutter



Figure 3: Weather clutter before adaption

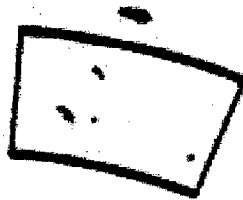


Figure 4: Weather clutter after adaption

2 Principle of air- and spaceborne MTI radar

In this section some important features of airborne clutter echoes are briefly discussed. The efficiency of space-time clutter suppression depends significantly on these properties. For definition of the geometry see Figure 5. It shows two important cases (sidelooking and forward looking arrays).

2.1 Effect of Platform Velocity

2.1.1 Models of clutter and target

The results presented in this paper have been calculated on the basis of simple models for target and interference. For the sake of brevity we give here only the models as used in the evaluation. For more details the reader is referred to [26, chapter 2].

Clutter

The $NM \times NM$ clutter covariance matrix has the form

$$\mathbf{Q} = \begin{pmatrix} \mathbf{Q}_{11} & \mathbf{Q}_{12} & \dots & \mathbf{Q}_{1M} \\ \mathbf{Q}_{21} & \mathbf{Q}_{22} & \dots & \mathbf{Q}_{2M} \\ \vdots & \vdots & \ddots & \vdots \\ \mathbf{Q}_{M1} & \mathbf{Q}_{M2} & \dots & \mathbf{Q}_{MM} \end{pmatrix} \quad (1)$$

where the indices of the submatrices m, p denote time (pulse repetition intervals) while the indices i, k run inside the submatrices and denote space (sensors). N is the number of sensors and M the number of coherently processed echoes. The elements of \mathbf{Q} are integrals over a full range circle

$$q_{ln}^{(c)} = P_c \int_{\varphi=0}^{2\pi} \rho_{mp} \rho_{i-k} \times D^2(\varphi) L^2(\varphi) G(\varphi, m) G^*(\varphi, p) \times \Phi_{m-p}^{(t)}(\varphi, v_p) \Phi_{i-k}^{(s)}(\varphi) d\varphi + P_N \quad (2)$$

$$m, p = 1 \dots M \quad i, k = 1 \dots N$$

where P_c is the clutter power at the single element at a certain instant of time and P_N the receiver noise power. The other symbols denote as follows: φ azimuth, s. Figure 5; A complex clutter amplitude; $D(\varphi)$ sensor directivity pattern; $L(\varphi)$ clutter reflectivity; ρ_{ik} spatial (sensor-to-sensor) correlation which is not considered here; ρ_{mp} temporal (echo-to-echo) correlation; $G(\varphi, m)$ transmit directivity pattern. The temporal and spatial phase terms are as follows

$$\Phi_m^{(t)}(\varphi) = \exp\left[j \frac{2\pi}{\lambda} 2v_p m T \cos \varphi \cos \theta\right]$$

$$\Phi_i^{(s)}(\varphi) = \exp\left[j \frac{2\pi}{\lambda} (x_i \cos \varphi + y_i \sin \varphi) \times \cos \theta - z_i \sin \theta\right] \quad (3)$$

The indices l, n of the $NM \times NM$ covariance matrix are related to the sensor indices i, k and echo indices m, p through

$$l = (m-1)N + i \quad m = 1 \dots M; \quad i = 1 \dots N \quad (4)$$

$$n = (p-1)N + k \quad p = 1 \dots M; \quad k = 1 \dots N \quad (5)$$

Noise

Receiver noise is assumed to be uncorrelated in space and time

$$E\{n_m n_p^*\} = \begin{cases} P_n & : m = p \\ 0 & : m \neq p \end{cases} \quad (6)$$

$$E\{n_i n_k^*\} = \begin{cases} P_n & : i = k \\ 0 & : i \neq k \end{cases} \quad (7)$$

where P_n denotes the white noise power.

Target

A target at azimuthal position φ_t moving at a radial velocity v_{rad} produces the following space-time signal at the array output

$$s_{mi}(\varphi_t) = A \exp\left[j \frac{2\pi}{\lambda} \times (2v_{rad} m T + (x_i \cos \varphi_t + y_i \sin \varphi_t) \cos \theta - z_i \sin \theta)\right] \quad (8)$$

$$m = 1 \dots M \quad i = 1 \dots N$$

2.1.2 The Isodops

Surfaces of constant Doppler are given by cones. Intersections of such cones with the planar ground results in a set of hyperbolas as shown in Figure 6 for horizontal flight and flat earth. The radar platform moves from left to right. Maximum Doppler is encountered at 0° (positive Doppler) and 180° (negative Doppler), zero Doppler at 90° 270° .

2.1.3 Impact of Array Geometry

Only one quadrant of the isodop field is shown in Figure 7 (thin curves).

The axis of a linear array in sidelooking orientation coincides with the flight path. Therefore, curves of constant look direction are again hyperbolas on the ground (fat curves). The beam traces of a linear sidelooking array coincide with the isodops. This means that the clutter Doppler is range independent. This important property has implications on clutter rejection.

The axis of a forward looking linear array is perpendicular to the flight axis. Therefore, the set of beam traces are rotated by 90° , s. Figure 8. Now one can notice that beam traces and isodops cross each other frequently. For a forward looking array the Doppler frequency of clutter echoes depends obviously on range. The range dependency occurs especially at short range, that is, where the range is of the order of magnitude of the platform height above ground.

2.1.4 Azimuth-Doppler Clutter Trajectories

Figure 9 shows the trajectories of clutter spectra in the azimuth² (abszissa) - Doppler (ordinate) plane. The four plots have been calculated for different crab angles ψ . For $\psi = 0^\circ$ (sidelooking array) all the clutter power is located on the diagonal of the plot while for increasing crab angle one obtains ellipses. Finally, $\psi = 90^\circ$ means a forward looking array, with the clutter power located on a circular trajectory.

Clutter echoes depend in general on range. First of all the backscattered clutter power decreases with range according to the radar equation: $P_c \propto \frac{1}{R^3}$.

² $\cos \varphi$

Doppler-range dependence

The range dependence of the clutter Doppler frequency has already been addressed in the context of isodops. It follows from the above considerations that the clutter Doppler is constant with range for a sidelooking array. Therefore, all four curves calculated for different ranges coincide (Figure 9a). From Figure 9d it is obvious that for a certain look direction the Doppler frequency increases with range in case of a forward looking array³.

2.2 Comparison of Spatial, Temporal and Space-Time Processing

The principle of space-time adaptive processing for clutter rejection in moving radars is illustrated in Figure 11. A sidelooking sensor configuration was assumed. The clutter spectrum extends along the diagonal of the $\cos \varphi - \omega_D$ plot. Notice the modulation by the transmit beam.

Conventional *temporal* processing means that the projection of the clutter spectrum onto the ω_D axis is cancelled via an inverse filter. Such filter is depicted in the back of the plot. As can be seen the clutter notch is determined by the projected clutter mainlobe which is a Doppler response of the transmit beam. Slow targets are attenuated.

Spatial processing as being used for jammer nulling requires that the clutter spectrum is projected onto the $\cos \varphi$ axis. Applying an inverse spatial clutter filter, however, forms a broad stop band in the look direction so that the radar becomes blind. Both fast and slow targets fall into the clutter notch.

Space-time processing exploits the fact that the clutter spectrum is basically a narrow ridge. A space-time clutter filter, therefore, has a two-dimensional *narrow* clutter notch so that even slow targets fall into the passband.

³This follows from the depression angle term $\cos \theta$ in (3).

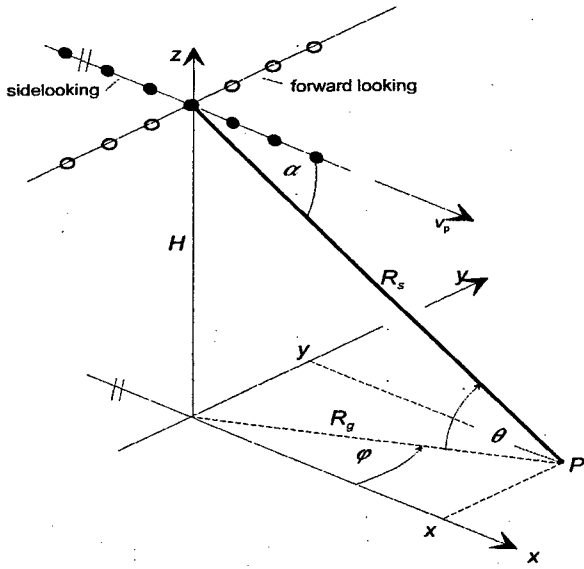


Figure 5: Geometry of airborne antenna arrays

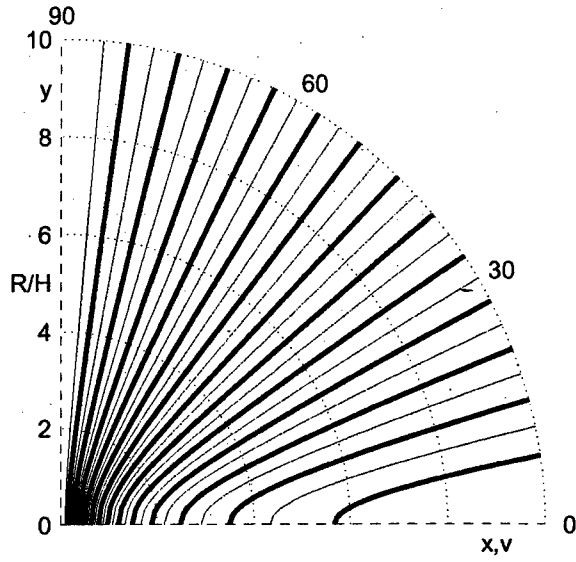


Figure 7: Beam traces (fat) and isodops for sidelooking array

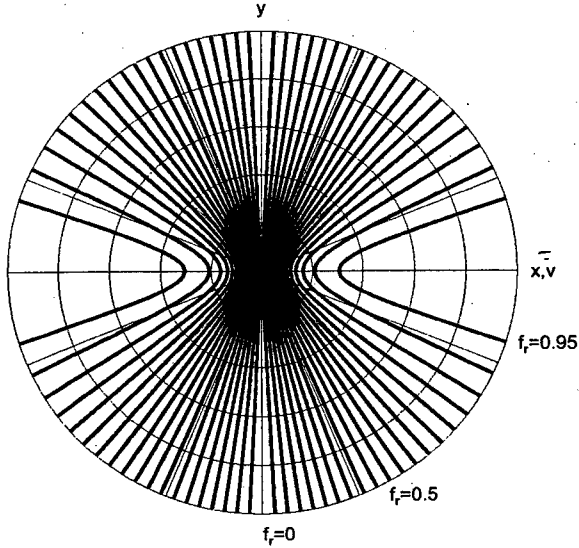


Figure 6: The isodops

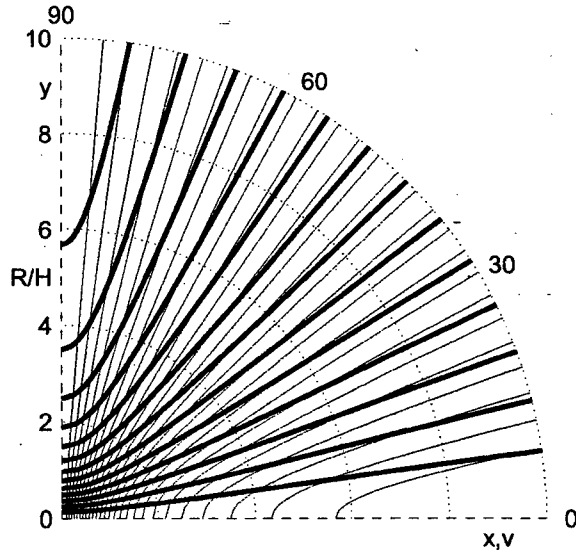


Figure 8: Beam traces (fat) and isodops for forward looking array

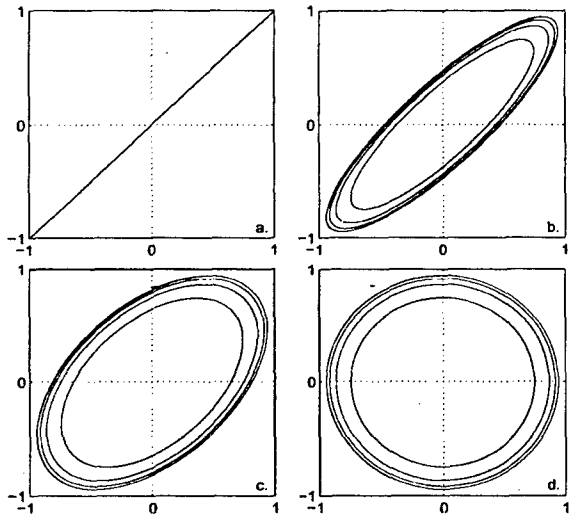


Figure 9: $f_r - \cos \varphi$ clutter trajectories for linear arrays: a. $\psi = 0^\circ$; b. $\psi = 30^\circ$; c. $\psi = 60^\circ$; d. $\psi = 90^\circ$; from inside to outside: $R/H = 1.5; 2; 2.5; 3$

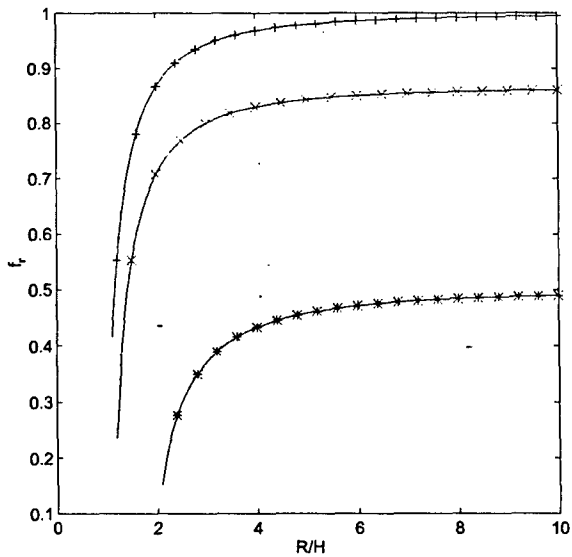


Figure 10: Range dependence of the clutter Doppler frequency for forward looking array: $+ \beta = 90^\circ$ (look direction=flight direction); $\times \beta = 60^\circ$; $* \beta = 30^\circ$

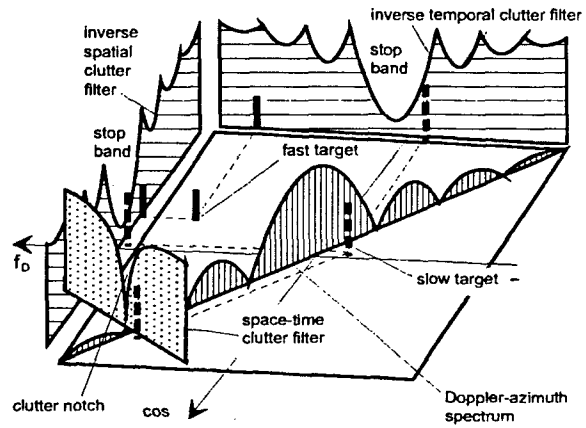


Figure 11: Principle of space-time clutter filtering (sidelooking array antenna)

3 Characteristics of Air- and Spaceborne Clutter

3.1 The Space-time Covariance Matrix

The space-time covariance matrix was defined in eqs. 1, 2. Figs. 12, 13 show the modulus of typical space-time covariance matrices. As can be seen from Fig. 12 the spatial submatrices are unity matrices with the diagonal shifted with the temporal indices M, p . In case of pure spatial processing we would deal with a $N \times N$ unity matrix only. In this case no substantial gain in clutter rejection can be achieved. Through spacetime processing we obtain the other correlation ridges in the matrix which provide the correlation required for clutter cancellation. If we use directive sensors and a directive transmit array some additional correlation comes up as can be seen in Fig. 13. Fig. 14 shows a space-time covariance matrix for noise jamming. As can be seen there is no temporal correlation.

3.2 Clutter Spectra

3.2.1 Eigenspectra

The concept of eigenanalysis of space-time clutter covariance matrices was introduced by the author [21]. The eigenspectrum (rank ordered sequence of eigenvalues) shows how large the clutter subspace is.

The elements of the space-time covariance matrix are calculated as

$$q_{ln} = E\{c_{im}c_{kp}^*\} + P_w\delta_{ikmp} \quad (9)$$

where c_{im} is the space-time clutter signal. The spatial (sensor) indices i, k and the temporal (echo pulse) indices m, p are related with the matrix indices through

$$l = (m-1)N + i \quad m = 1 \dots M; \quad i = 1 \dots N \quad (10)$$

$$n = (p-1)N + k \quad p = 1 \dots M; \quad k = 1 \dots N \quad (11)$$

P_w is the receiver noise power and δ_{ikmp} the Kronecker symbol. It was found in [21] that for a sidelooking equidistant array and the PRF chosen so that DPCA conditions are fulfilled (see section 4.1.1) the number of eigenvalues is

$$N_e = N + M - 1.$$

This figure determines the minimum size of the number of degrees of freedom of the space-time clutter filter.⁴

3.2.2 Power Spectra

Based on the space-time clutter+noise covariance matrix azimuth-Doppler spectra can be generated, either by 2D Fourier transform of the covariance matrix, or by use of one of the well-known high resolution power estimators.

Let us consider a covariance matrix of the form

$$\mathbf{R} = E\{\mathbf{x}\mathbf{x}^*\} = \mathbf{S} + \mathbf{N} \quad (12)$$

where \mathbf{N} is the noise component and \mathbf{S} includes all kind of signal or interference. Then the output of a signal matched filter is simply

$$y_{SM}(\Theta) = \mathbf{x}^*\mathbf{s}(\Theta) \quad (13)$$

and the normalised power output is

$$P_{SM}(\Theta) = \frac{\mathbf{s}^*(\Theta)\mathbf{R}\mathbf{s}(\Theta)}{\mathbf{s}^*(\Theta)\mathbf{s}(\Theta)} \quad (14)$$

⁴Actually in [21] it reads $N_e = N + M$. The correct number is $N_e = N + M - 1$.

$s(\Theta)$ is a steering vector which seeks for signal components $s(\Theta_i)$ in \mathbf{R} . $P(\Theta)$ attempts to become maximum wherever the steering vector $s(\Theta)$ coincides with a signal vector $s(\Theta_i)$ in \mathbf{R} . For sinusoidal signals the signal matched filter becomes the 2D Fourier transform.

Fig. 18 shows a 2D Fourier clutter spectrum. One recognises the main beam response and the sidelobe response along the diagonal. In addition there are spurious Doppler and azimuthal sidelobes which are responses of the spatial and temporal FT to the main beam clutter. Notice that only the clutter along the diagonal is physical clutter, the sidelobes along the Doppler and azimuth axes are artifacts. Similar relations can be observed if Hamming weighting is applied in space and time (Fig. 19).

The minimum variance estimator has proven to be the most useful because its response is closest to the clutter contained in the covariance matrix. In analogy with (19) the minimum variance estimator becomes

$$\bar{\mathbf{w}}_{MV} = \gamma \mathbf{R}^{-1} \mathbf{s} \quad (15)$$

with $\gamma = (\mathbf{s}^* \mathbf{R}^{-1} \mathbf{s})^{-1}$. The output power is

$$P_{MV}(\Theta) = (\mathbf{s}^*(\Theta) \mathbf{R}^{-1} \mathbf{s}(\Theta))^{-1} \quad (16)$$

Figures 20 and 21 show typical MV clutter spectra (F is the normalised Doppler frequency) for sideways and forward looking linear arrays. For the sidelooking array the clutter power is distributed on the diagonal⁵ of the plot while in case of a forward looking configuration the clutter is distributed on a semi-circle. Notice that in this example the individual sensors have sensor patterns which blank the rear semi-plane out. Otherwise the clutter power of the forward looking array would be distributed on a full circle.

⁵The wavy shape of the trajectory is due to the fact that we used φ instead of $\cos \varphi$ for the abszissa.

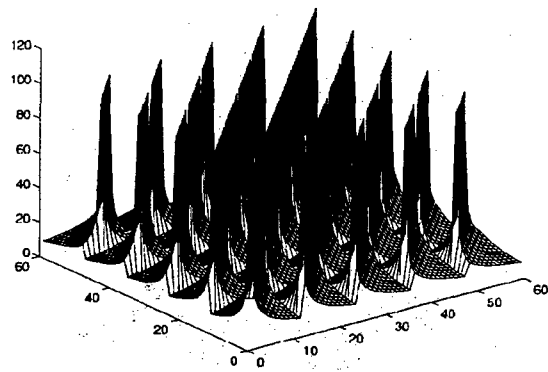


Figure 12: Modulus of the clutter covariance matrix vs horizontal and vertical index (sidelooking linear array, $N=12$, $M=5$, omnidirectional sensors and transmission)

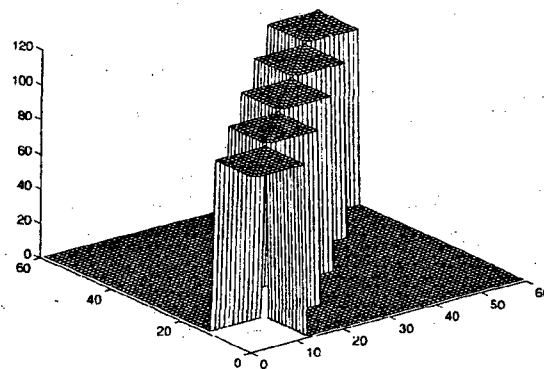


Figure 14: Jammer covariance matrix (sidelooking array, $N=12$, $M=5$, 1 jammer, absolute values)

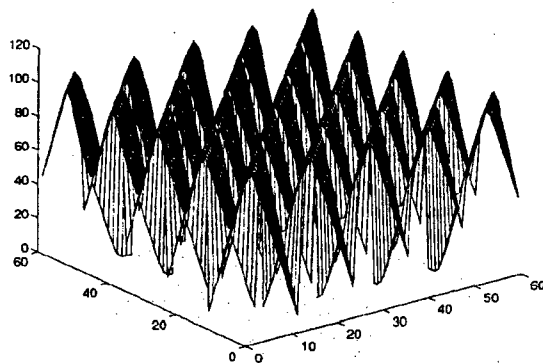


Figure 13: Modulus of the clutter covariance matrix vs horizontal and vertical index (sidelooking linear array, $N=12$, $M=5$, directive sensors and transmission)

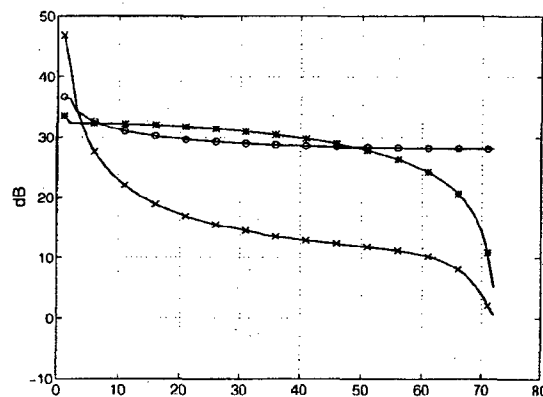


Figure 15: Eigenspectra of a spatial covariance matrix. $N = 72$, $M = 1$; \circ omnidirectional sensors and transmission; $*$ directive sensors; \times directive sensors and transmission

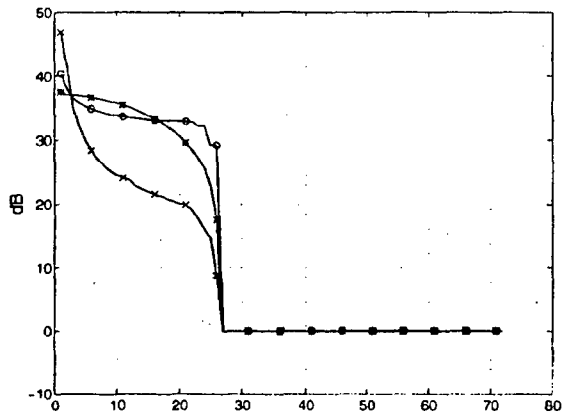


Figure 16: Eigenspectra of a *space-time* covariance matrix (sidelooking array). $N = 24$, $M = 3$; \circ omnidirectional sensors and transmission; $*$ directive sensors; \times directive sensors and transmission

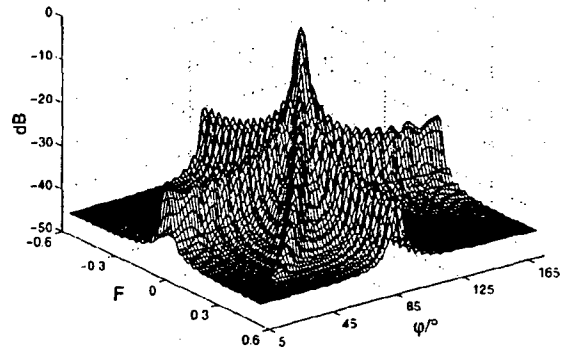


Figure 18: Fourier clutter spectrum (sidelooking array, $\varphi_L = 90^\circ$)

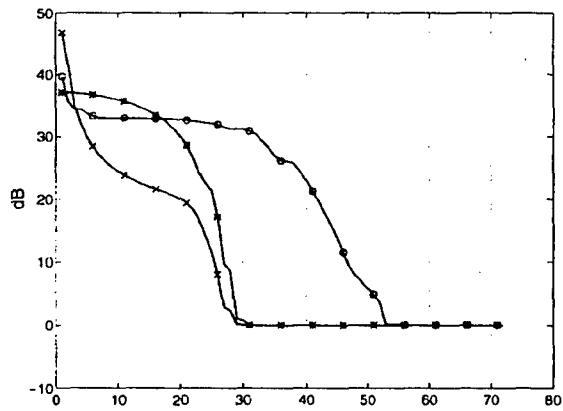


Figure 17: Eigenspectra of a *space-time* covariance matrix (forward looking array). $N = 24$, $M = 3$; \circ omnidirectional sensors and transmission; $*$ directive sensors; \times directive sensors and transmission

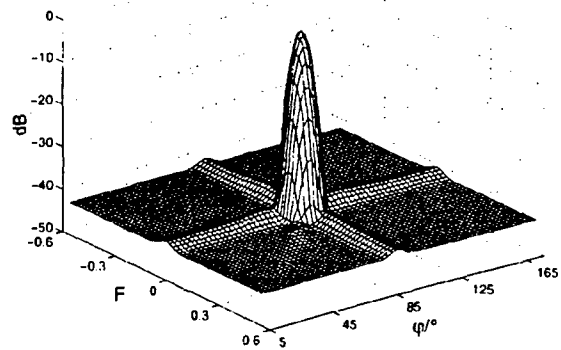


Figure 19: Fourier clutter spectrum with spatial and temporal Hamming weighting (sidelooking array, $\varphi_L = 0^\circ$)

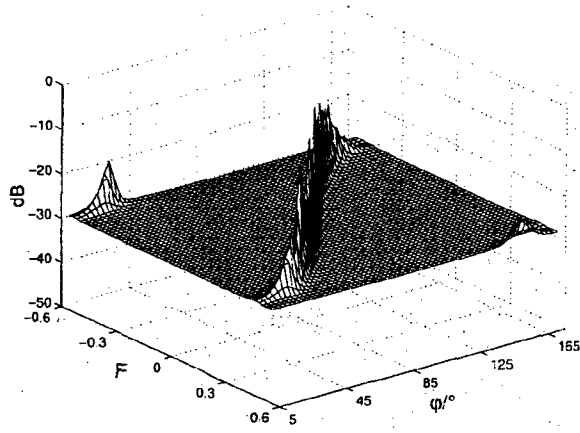


Figure 20: MV clutter spectrum (sidelooking array, $\phi_L = 45^\circ$)

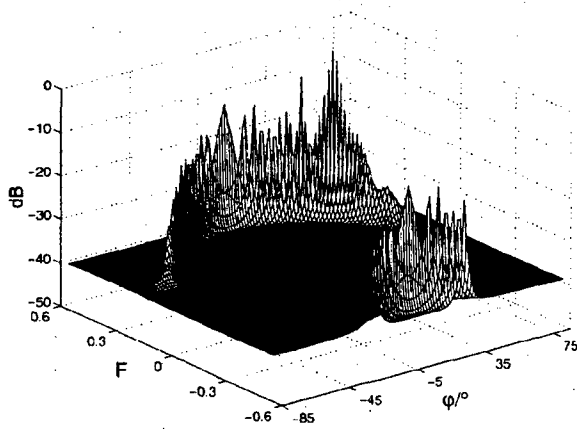


Figure 21: MV spectrum for forward looking linear array

4 The Optimum Space-Time Processor

4.1 Historical: The Displaced Phase Center Antenna (DPCA)

4.1.1 The DPCA technique

DPCA (displaced phase centre antenna) is a technique which compensates physically for the motion of the radar platform to reduce the effect of motion induced Doppler spread of clutter returns. Consider two antennas in sidelooking configuration as shown in Figure 22. At time $m = 1$ they assume the dashed position, at time $m = 2$ the solid one. As can be noticed the first antenna at $m = 1$ assumes the position of the second sensor at time $m = 2$. This is equivalent to having one antenna fixed in space⁶ for the duration of one pulse interval. Clutter suppression is done by subtracting so that the clutter remainder becomes $\epsilon = q_2 - c_{21}$. If $c_{12} = c_{21}$ perfect cancellation is obtained. Notice that this technique was implemented in RF technology long time before the age of digital signal processing.

4.1.2 A note on DPCA and STAP

For more than 3 decades the DPCA principle (motion compensation by spatial coincidence of sensor positions, s. section 4.1.1 and Figure 22) has been considered the physical background of space-time clutter rejection. More recently, numerical investigations have shown that forward looking arrays (which do not have the DPCA property) work as well with space-time adaptive processing.

This reveals that the function of STAP is not based on a DPCA geometry. The space-time filtering is just based on the fact that airborne clutter echoes are signals depending on the two variables space and time, and they are *bandlimited* in the Doppler as well as in the azimuth dimension. If such signals are properly sampled in space (sensor displacement) and time (PRF) any kind of filtering can basically be applied without aliasing losses. The property of slow target detection is based on the special shapes of such clutter spectra (narrow ridge). STAP is not based on DPCA. DPCA is merely a special case of STAP. The DPCA property plays a role in the context of compensating for the effects of system bandwidth.

4.2 The LR-Test for 2-D Vector Quantities

The principle of detecting a signal vector \mathbf{s} before a noisy background given by \mathbf{q} is briefly summarized. Let us define the following complex vector quantities:

$$\mathbf{q} = \begin{pmatrix} \mathbf{q}_1 \\ \mathbf{q}_2 \\ \vdots \\ \mathbf{q}_N \end{pmatrix}; \quad \mathbf{s} = \begin{pmatrix} s_1 \\ s_2 \\ \vdots \\ s_N \end{pmatrix}; \quad \mathbf{x} = \begin{pmatrix} \mathbf{x}_1 \\ \mathbf{x}_2 \\ \vdots \\ \mathbf{x}_N \end{pmatrix} \quad (17)$$

where $\mathbf{q}_m, \mathbf{s}_m$ and \mathbf{x}_m are the spatial subvectors (signals at the array output) at the m -th pulse repetition interval. In general the noise vector consists of a correlated part \mathbf{c} (e.g. jammer, clutter) and an uncorrelated part \mathbf{n} (e.g. receiver noise):

$$\mathbf{q} = \mathbf{c} + \mathbf{n} \quad (18)$$

The signal vector \mathbf{s} is assumed to be deterministic. \mathbf{x} is the actual data vector which may be noise only ($\mathbf{x} = \mathbf{q}$) or signal-plus-noise ($\mathbf{x} = \mathbf{q} + \mathbf{s}$). The problem of extracting \mathbf{s} optimally out of the background noise \mathbf{q} is solved by applying the well-known linear weighting

$$\mathbf{w}_{\text{opt}} = \gamma \mathbf{Q}^{-1} \mathbf{s} \quad (19)$$

⁶Due to the factor of 2 in the Doppler term $2mv_p T$ the antenna motion during one PRI is only half the antenna spacing. It is important that phase coincidence of clutter echoes occurs.

A block diagram of the optimum processor is shown in Fig. 23. The spatial dimension is given by the N antenna elements while the temporal dimension is given by shift registers where M subsequent echoes are stored. These space-time data are multiplied with the inverse of the space-time adaptive clutter covariance matrix for clutter cancellation. The output signal are then fed into a space-time weighting network whose coefficients form a space-time replica (beamformer and Doppler filter) of the desired signal.

4.2.1 Performance of the Optimum Processor

The efficiency of any linear processor w can be characterized by the improvement factor⁷ which is defined as the ratio of signal-to-noise power ratios at output and input, respectively

$$IF = \frac{\frac{P_s^{out}}{P_n^{out}}}{\frac{P_s^{in}}{P_n^{in}}} = \frac{\frac{w^* s s^* w}{w^* Q w}}{\frac{s^* s}{\text{tr}(Q)}} = \frac{w^* s s^* w \cdot \text{tr}(Q)}{w^* Q w \cdot s^* s} \quad (20)$$

Figs. 24 and 25 show examples for the improvement factor in the azimuth-Doppler plane for sidelooking and forward looking linear arrays. Along the clutter trajectory we have now a clutter notch.

4.2.2 Comparison with 1-dimensional Methods

The question is, how much is the advantage of space-time processing versus conventional techniques. Such a comparison has been made in Fig. 26. The optimum space-time processor is compared with a beamformer cascaded with an optimum temporal clutter filter, and simple Beamforming plus Doppler filtering. The advantage of space-time processing is obvious.

4.2.3 Range-Doppler Matrix

Plotting clutter power or IF versus Doppler and range results in the range-Doppler Matrix. Figures 27 and 28 show examples for sidelooking and forward looking. For sidelooking radar (Figure 27) the clutter trajectory is a straight vertical line which corresponds to the fact that the clutter Doppler is range independent, compare with Figure 7. For forward looking radar we notice a certain dependency of the clutter Doppler with range, especially at short range, which is consistent with Figure 8.

4.3 Optimum Processor and Eigencanceller

The Eigencanceller is a zero noise approximation of the optimum processor. It is given by

$$P = I - E(E^*E)^{-1}E^* \quad (21)$$

where E is the matrix of eigenvectors belonging to the interference component in Q . Figure 29 shows a comparison of the optimum processor and the eigencanceller. The curves are almost identical, except for the clutter notch. Here the optimum processor suppresses the interference down to the noise level whereas the eigencanceller forms an exact null. The eigencanceller needs less training data for adaptation than the optimum processor which can be a significant advantage for real-time operation.

⁷The expression *improvement factor* is commonly used for characterizing *temporal* (i.e., pulse-to-pulse) filters for clutter rejection. The same formula may be used for *spatial* applications (array processing) in the context of interference or jammer suppression. Then instead of *improvement factor* the term *gain* is used. Since our main objective is clutter rejection we prefer the term *improvement factor* or its abbreviation IF.

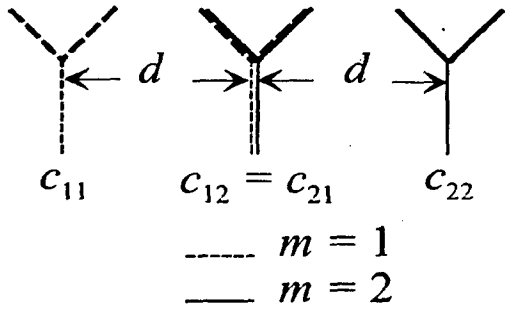


Figure 22: Principle of a 2-pulse DPCA clutter canceller

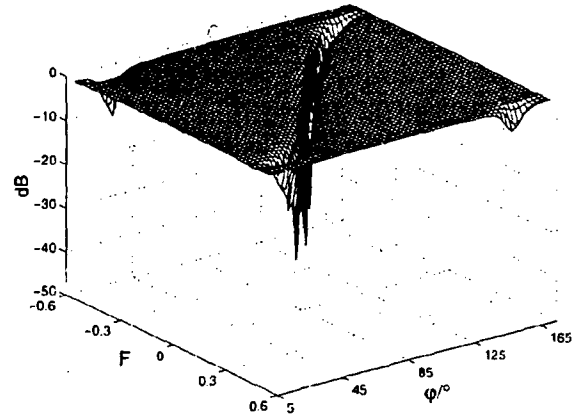


Figure 24: Improvement factor for sidelooking array

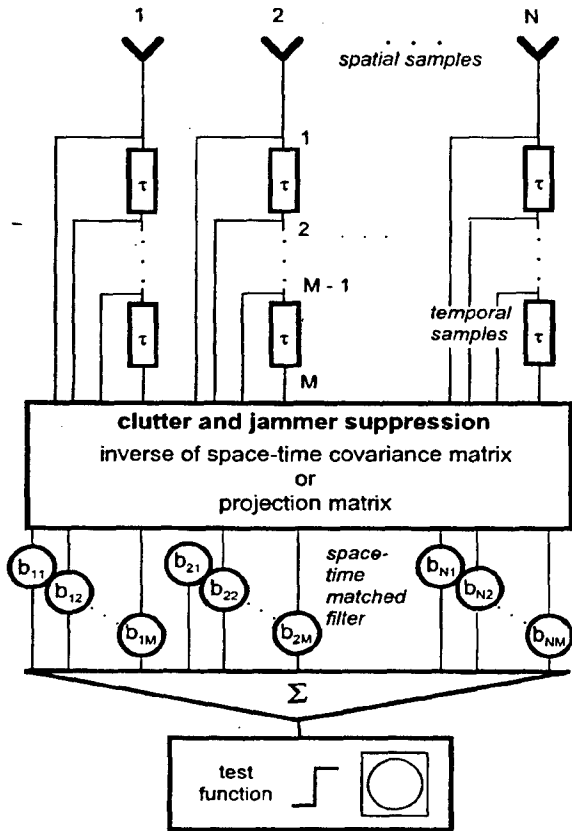


Figure 23: The optimum adaptive space-time processor

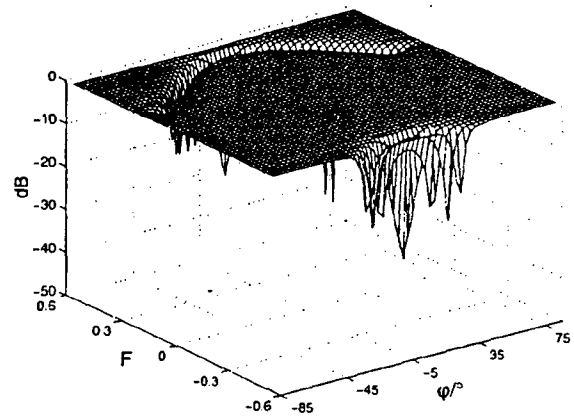


Figure 25: Improvement factor for forward looking array

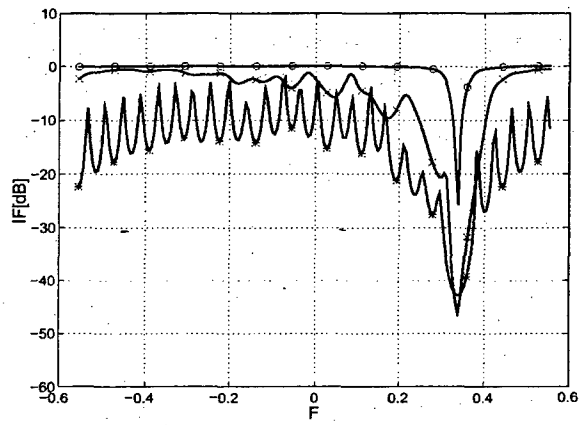


Figure 26: The potential of space-time adaptive processing: o optimum processing; * beamformer + Doppler filter; x beamformer + adaptive temporal filter

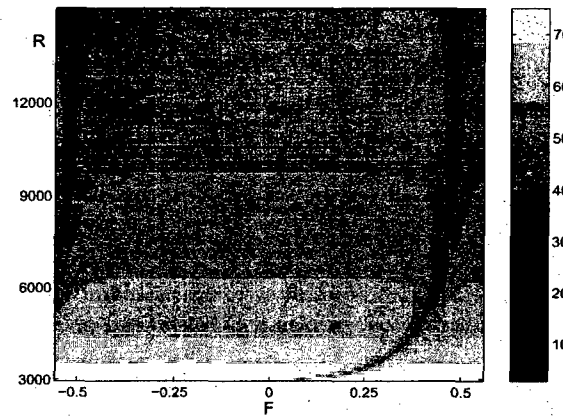


Figure 28: Range-Doppler Matrix (greytones denote IF/dB, $R = \text{range/m}$, $\varphi_L = 0^\circ$)

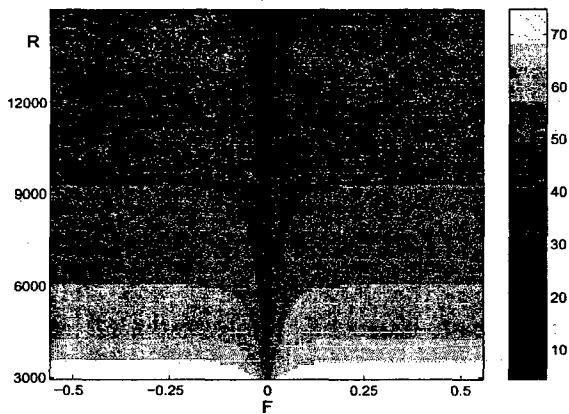


Figure 27: Range-Doppler Matrix (greytones denote IF/dB, $R = \text{range/m}$, $\varphi_L = 90^\circ$)

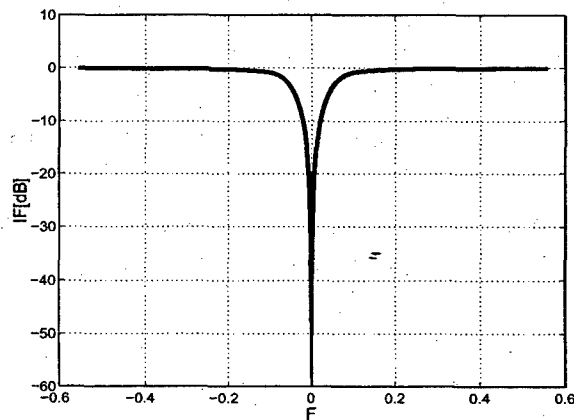


Figure 29: Comparison of optimum and orthogonal projection processing

References

- [1] Anderson, D. B., "A Microwave Technique to Reduce Platform Motion and Scanning Noise in Airborne Moving Target Radar", *IRE WESCON Com. Record*, Vol. 2, pt. 1, 1958, pp. 202-211
- [2] Babu, S. B. N., Torres, J. A., Lamensdorf, D., "Space-Time Adaptive Processing for Airborne Phased Array Radar, *Proc. of the Conf. on Adaptive Antennas*, 7-8 November 1994, McIlville, New York 11747, pp. 71-75
- [3] Brennan, L. E., Reed, I. S., "Theory of Adaptive Radar", *IEEE Trans. AES*, Vol. 9, No 2, March 1973, pp. 237-252
- [4] Brennan, L. E., Mallett, J. D., Reed, I. S., "Adaptive Arrays in Airborne MTI", *IEEE Trans. AP*, Vol. 24, No. 5, 1976, pp. 607-615
- [5] Brennan, L. E., Staudaher, F. M., "Subclutter Visibility Demonstration", *Technical Report RL-TR-92-21, Adaptive Sensors Incorporated*, March 1992
- [6] Bühring, W., Klemm, R., "Ein adaptives Filter zur Unterdrückung von Radarstörungen mit unbekanntem Spektrum" (An adaptive filter for suppression of clutter with unknown spectrum), *FREQUENZ*, Vol. 30, No. 9, September 1976, (in German), pp. 238-243
- [7] Coe, D. J., White, R. G., "Experimental moving target detection results from a three-beam airborne SAR", *AEU*, Vol. 50, No. 2, March 1996
- [8] Compton, R. T. jr., "The Bandwidth Performance of a Two-Element Adaptive Array with Tapped Delay-Line Processing", *IEEE Transaction on Antenna and Propagation*, Vol. AP-36, No. 1, January 1988, pp. 5-14
- [9] Compton, R. T. jr., "The Relationship Between Tapped Delay-Line and FFT Processing in Adaptive Arrays", *IEEE Transaction on Antenna and Propagation*, Vol. AP-36, No. 1, January 1988, pp. 15-26
- [10] Covault, C., "Space-based radars drive advanced sensor technologies", *Aviation Week & Space Technology*, April 5, 1999, pp. 49-50
- [11] Doherty, J. F., "Suppression of Terrain Scattered Jamming in Pulse Compression Radar", *IEEE Transactions on Signal Processing*, Vol. 2, No. 1, January 1995, pp. 4-6
- [12] Ender, J., "The airborne experimental multi-channel SAR system", *Proc. EUSAR '96*, 26-28 March 1996, Koenigswinter, Germany, pp. 49-52 (VDE Publishers)
- [13] Ender, J., "Detection and Estimation of Moving Target Signals by Multi-Channel SAR", *Proc. EUSAR '96*, 26-28 March 1996, Koenigswinter, Germany, pp. 411-417, (VDE Publishers). Also: *AEU*, Vol. 50, March 1996, pp. 150-156
- [14] Ender, J., "Experimental results achieved with the airborne multi-channel SAR systems AER II. The airborne experimental multi-channel SAR system", *Proc. EUSAR '98*, 25-27 May 1998, Friedrichshafen, Germany
- [15] Farina, A., Timmoneri, L., "Space-time processing for AEW radar", *Proc. RADAR 92*, Brighton, UK, 1992, pp. 312-315
- [16] Gross, L.A., Holt, H.D., "AN/APY-6 realtime surveillance and targeting radara development", *Proc. NATO/IRIS Conference*, 19-23 October 1998, paper G-3
- [17] Haimovich, A. L., Bar-Ness, Y., "An Eigenanalysis Interference Canceler", *IEEE Trans. Signal Processing*, Vol. 39, No. 1, January 1991, pp. 76-84

- [18] Ayoub, T. F., Haimovich, A. M., Pugh, M. L., "Reduced-rank STAP for high PRF radar", *IEEE Trans. AES*, Vol. 35, No. 3, July 1999, pp. 953-962
- [19] Hippler, J., Fritsch, B., "Calibration of the Dornier SAR with trihedral corner reflectors", *Proc. EU-SAR '96*, 26-28 March 1996, Koenigswinter, Germany, pp. 499-503, (VDE Publishers)
- [20] Jouny, I. I., Culpepper, E., "Modeling and mitigation of terrain scattered interference", *IEEE Antennas and Propagation Symposium*, 18-23 June, 1995, Newport Beach, USA, pp. 455-458
- [21] Klemm, R., "Adaptive Clutter Suppression for Airborne Phased Array Radar", *Proc. IEE*, Vol. 130, No. 1, February 1983, pp. 125-132
- [22] Klemm, R., Ender, J., "New Aspects of Airborne MTI", *Proc. IEEE Radar 90*, Arlington, USA, 1990, pp. 335-340
- [23] Klemm, R., "Antenna design for airborne MTI", *Proc. Radar 92*, October 1992, Brighton, UK, pp. 296-299
- [24] Klemm, R., "Adaptive Airborne MTI: Comparison of Sideways and Forward Looking Radar", *IEEE International Radar Conference*, Alexandria, VA, May 1995, pp. 614-618
- [25] Klemm, R., ed., *Digest of the IEE Colloquium on STAP*, 6 April 1998, IEE, London, UK
- [26] Klemm, R., *Space-Time Adaptive Processing - Principles and Applications* IEE Publishers, London, UK, 1998)
- [27] Klemm, R., "Comparison between monostatic and bistatic antenna configurations for STAP", *IEEE Trans. AES*, April 2000
- [28] Klemm, R., (ed.), Special issue on "Space-Time Adaptive Processing", *IEE ECEJ*, February 1999
- [29] Klemm, R., "Space-time adaptive FIR filtering with staggered PRI", *ASAP 2001*, MIT Lincoln Lab., Lexington, MA, USA, 13-15 March 2001, pp.
- [30] Klemm, R., "Doppler properties of airborne clutter", *RTO SET Lecture Series 228* (this volume)
- [31] Koch, W., Klemm, R., "Ground target tracking with STAP radar", *IEE Proc. Radar, Sonar and Navigation*, 2001
- [32] Melvin, W. L., (ed.), Special issue on "Space-Time Adaptive Processing and Adaptive Arrays", *IEEE Trans. AES*, April 2000
- [33] Kreyenkamp, O., "Clutter covariance modelling for STAP in forward looking radar", *DGON International Radar Symposium 98*, September 15-17, 1998, München, Germany
- [34] Lee, F. W., Staudaher, F., "NRL Adaptive Array Flight Test Data Base", *Proc. of the IEEE Adaptive Antenna Systems Symposium*, Melville, New York, November 1992
- [35] Richardson, P. G., Hayward, S. D., "Adaptive Space-Time Processing for Forward Looking Radar", *Proc. IEEE International Radar Conference*, Alexandria, VA, USA, 1995, pp. 629-634
- [36] Richardson, P. G., "Effects of manoeuvre on space-time adaptive processing performance", *Proc. IEE Radar '97*, 14-16 October 1997, Edinburgh, Scotland, pp. 285-289
- [37] Sanyal, P. K., Brown, R. D., Little, M. O., Schneible, R. A., Wicks, M. C., "Space-time adaptive processing bistatic airborne radar", *IEEE National Radar Conference*, 20-22 April 1999, Boston, USA, pp. 114-118

- [38] Shnitkin, H., "A Unique JOINT STARS Phased Array Antenna", *Microwave Journal*, January 1991, pp. 131-141
- [39] Skolnik, M., *Radar Handbook*, 1st Ed., McGraw-Hill, New York, 1970
- [40] Tobin, M., "Real-Time Simultaneous SAR/GMTI in a Tactical Airborne Environment", *Proc. EUSAR '96*, 26-28 March, 1996, Koenigswinter, Germany, pp. 63-66, (VDE Publishers)
- [41] Titi, G. W., "An Overview of the ARPA/NAVY Mountaintop Program", *IEEE Adaptive Antenna Symposium*, Melville, New York November 7-8, 1994
- [42] Tsandoulas, G. N., "Unidimensionally Scanned Phased Arrays", *IEEE Trans. on Antennas and Propagation*, Vol. AP28, No. 1, November 1973, pp. 1383-1390
- [43] Wang, H., Cai, L., "On Adaptive Spatial-Temporal Processing for Airborne Surveillance Radar Systems", *IEEE Trans. AES*, Vol. 30, No. 3, July 1994, pp. 660-670
- [44] Wang Z., Bao Z., "A Novel Algorithm for Optimum and Adaptive Airborne Phased Arrays", *Proc. SITA '87*, 19-21 November 1987, Tokyo, Japan, pp. EE2-4-1
- [45] Wang, H., Zhang, Y., Zhang, Q., "An Improved and Affordable Space-Time Adaptive Processing Approach", *Proc. International Conference on Radar (ICR '96)*, Beijing, China, 8-10 October 1996, pp. 72-77
- [46] Ward, J., "Space-Time Adaptive Processing for Airborne Radar", *Technical Report No. 1015*, Lincoln Laboratory, MIT, December 1994
- [47] Ward, J., "Cramer-Rao Bounds for Target Angle and Doppler Estimation with Space-Time Adaptive Processing Radar", *Proc. 29th ASILOMAR Conference on Signals, Systems and Computers*, 30 October-2 November 1995, pp. 1198-1203